J Mater Sci (2016) 51:5403–5411

Synthesis and photoluminescence properties of $Ba_3Al_2O_6:Eu^{3+}$ red phosphor

Weixiong You[1,*], Zongliang Xiao[1], Fengqin Lai[1], Xinyu Ye[2], Qian Zhang[1], Honghui Jiang[1], Chunxiang Wang[1], Jinsheng Liao[1], Xiaolin Liu[1], and Shengwen Zhong[1]

[1] School of Material Science and Engineering, Jiangxi University of Science and Technology, Ganzhou 341000, People's Republic of China

[2] School of Metallurgy and Chemistry Engineering, Jiangxi University of Science and Technology, Ganzhou 341000, People's Republic of China

Received: 31 August 2015
Accepted: 19 February 2016
Published online: 1 March 2016

ABSTRACT

Eu^{3+}-doped $Ba_3Al_2O_6$ red phosphors were synthesized by high-temperature solid-state reaction. The crystal structure, morphology and luminescence properties were investigated by XRD, TEM and photoluminescence spectroscopy. The effect of calcination temperature, Eu^{3+} concentration as well as charge compensators on the luminescence properties was also investigated. Characteristic orange-red emission at 589 nm was detected under 394 nm excitation. The best performance could be derived for the sample calcined at 1450 °C. With the increase of Eu^{3+} concentration, the emission intensities increased gradually up to the Eu^{3+} concentration of 12 %. The emission intensities could be enhanced with Li^+, Na^+ and K^+ introduced as charge compensators. The results showed that $Ba_3Al_2O_6:Eu^{3+}$ phosphors with charge compensator had potential application in the fields of near-UV-excited WLEDs.

Introduction

Recently, white light-emitting diodes (WLEDs) have attracted much attentions due to its compactness, high efficiency, long operational lifetime, energy saving and environment protection [1–4]. However, the commercial WLEDs fabricated using yellow-emitting $YAG:Ce^{3+}$ phosphors with blue LED chips have a notable deficiency because of the scarcity of red emission, restricting their applications in some important fields, especially in lighting markets [5]. Nowadays, near-UV LED chips coated with red, green and blue phosphors are considered as a potential system to produce better properties in emission efficiency, colour temperature and colour rendering index [6, 7]. Comparing with the blue and green phosphors, the commonly used red phosphors for WLEDs show lower chemical stabilities and fluorescence efficiencies. Therefore, stable and high-efficient red phosphors suitable for near-UV chips are necessary for the development of WLEDs.

Among all the host materials used in WLEDs, rare earth-doped Alkaline earth aluminates $M_3Al_2O_6$ (M = Ca, Sr, Ba) possess many advantages, such as

Address correspondence to E-mail: you_wx@126.com

DOI 10.1007/s10853-016-9843-5

high chemical stability, high luminescence intensity, high quantum efficiency, nontoxic, low cost and so on [8]. The structure of $M_3Al_2O_6$ belongs to the cubic system with space group Pa3 [9–11]. M has six independent crystallographic sites in $M_3Al_2O_6$ lattices [12]. Recently, it is reported that Eu^{3+}- or Dy^{3+}-doped $Ca_3Al_2O_6$ and Eu^{2+}-doped $Sr_3Al_2O_6$ can be used as promising phosphors for fabrication of warm WLED [13–15]. In addition, $Ca_3Al_2O_6$ and $Sr_3Al_2O_6$ are popular hosts in $M_3Al_2O_6$ system and the luminescence properties of rare earth ions doped in these two hosts have been investigated [8, 16, 17]. But to our best knowledge, there are few reports on the photoluminescence properties of rare earth-doped $Ba_3Al_2O_6$. In this work, the Eu^{3+}-doped $Ba_3Al_2O_6$ phosphors are prepared by the method of high-temperature solid-state reaction. The luminescence properties of $Ba_3Al_2O_6$:Eu^{3+} are investigated, and the effect of calcinations temperature, Eu^{3+} concentration as well as charge compensations on the luminescence properties is also discussed.

Experiment

$Ba_3Al_2O_6$:Eu^{3+} phosphor was synthesized by high-temperature solid-state method using Eu_2O_3 (99.99 %), $BaCO_3$ (AR), Al_2O_3 (AR), Li_2CO_3 (AR), Na_2CO_3 (AR) and K_2CO_3 (AR) as reagents. Two types of samples were prepared: $Ba_3Al_2O_6$:xEu^{3+}($x = 0.02$, 0.04,…, 0.16), $Ba_3Al_2O_6$:$0.06Eu^{3+}$, $0.06Z$ ($Z = Li^+$, Na^+, K^+). According to the formula above, stoichiometric amounts of starting materials were weighed and then mixed thoroughly in the agate mortar. The mixture was calcined at different temperatures (1300, 1350, 1400 and 1450 °C) in a muffle furnace in air atmosphere for about 6 h. After cooling down to room temperature, white powder samples were obtained and then reground.

X-ray diffraction patterns of the samples in the range of $10° \leq 2\theta \leq 90°$ were recorded on a Bruker D8 Advance X-ray diffractometer with Cu K_α radiation ($\lambda = 1.54178$ Å). Transmission electron microscopy (TEM) micrographs were taken with a Tecnai G2 F20 field-emission transmission electron microscope. The excitation and emission spectra of the samples were detected by Hitachi F-7000 fluorescence spectrometer. The light source was xenon lamp and resolution was 0.5 nm. The light emitted from the Xe lamp entered the excitation side monochromator and then incident on the sample. Luminescence signal emitted from the sample directed into the emission side monochromator and was condensed onto the photomultiplier tube by concave mirror, whereby its intensity was measured. To ensure the identical measurement conditions of photoluminescence spectra for the different samples, the slit width, scan speed and high voltage of photomultiplier tube were kept unchanged for each measurement. All measurements were carried out at room temperature and the spectra had been corrected.

Results and discussion

Photoluminescence characteristics

The photoluminescence spectra of $Ba_3Al_2O_6$:$0.06Eu^{3+}$ calcined at 1450 °C are presented in Fig. 1. In the excitation spectrum found in Fig. 1a, there are broadband centred at about 270 nm associated with the charge transfer (CT) transition from 2p orbital of O^{2-} ions to 4f orbital of Eu^{3+} ions and narrower bands arising from intraconfigurational 4f–4f transitions (assignment is given in Figure). The emission spectrum of $Ba_3Al_2O_6$:$0.06Eu^{3+}$ sample under 394 nm excitation (Fig. 1b) consists of two emission bands with peaks at 589 and 612 nm, corresponding to the $^5D_0 \rightarrow {}^7F_1$ and $^5D_0 \rightarrow {}^7F_2$ transitions. The most intense peak located at 589 nm confirms that Eu^{3+} ion occupies the lattice site with inversion centre of symmetry [18, 19].

The effect of calcination temperature on the photoluminescence properties of $Ba_3Al_2O_6$:$0.06Eu^{3+}$

The XRD patterns of $Ba_3Al_2O_6$:$0.06Eu^{3+}$ calcined at four different temperatures are shown in Fig. 2. It can be seen from the figure that all the diffraction peaks of samples show very similar profiles and they are in agreement with that of the standard card (JCPDS No. 25-0075), which means that cubic phase $Ba_3Al_2O_6$ is predominant in the samples. Some additional peaks at about 22.5° and 36.2° are observed for the samples with calcination temperature 1300 and 1350 °C in Fig. 2. These additional peaks maybe attributed to the diffraction of $BaCO_3$ (JCPDS No.52-1528). The decomposition temperature of $BaCO_3$ is 1300 °C, so it may not be decomposed completely at 1300 and 1350 °C because of the temperature fluctuation in the

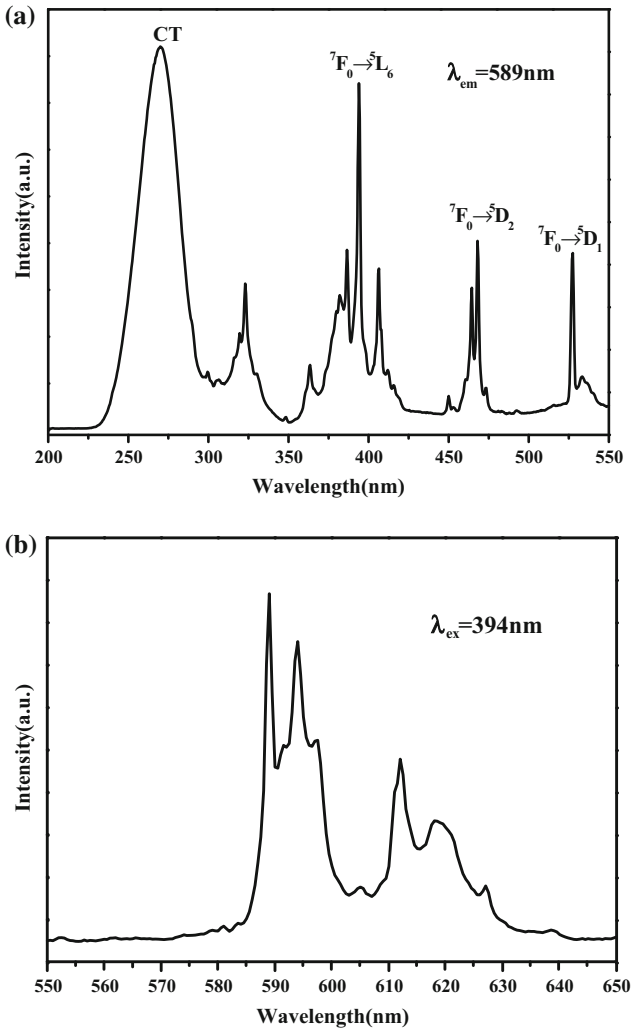

Figure 1 The photoluminescence spectra of $Ba_3Al_2O_6$:0.06Eu^{3+} calcined at 1450 °C. **a** Excitation spectrum measured while detecting the emission line at 589 nm; **b** emission spectrum measured under 394 nm excitation.

furnace. The intensities of diffraction peaks increase when the calcination temperature increases from 1300 to 1450 °C, which indicates that higher crystalline is obtained at higher calcination temperature.

Figure 3 shows the TEM images of $Ba_3Al_2O_6$:0.06-Eu^{3+} calcined at different temperatures. It is found that the morphology of the sample depends on the calcination temperature heavily. The particles of sample calcined at 1300 °C are irregular with sizes in the range of 40–60 nm and aggregated evidently, as shown in Fig. 3a and b. The high-resolution TEM (HRTEM) image exposes the crystalline nature of the sample. In Fig. 3c, lattice fringes can be observed and the interplanar spacing is 0.375 nm, indexed to be (331) planes. However, most of the fringes cannot be observed

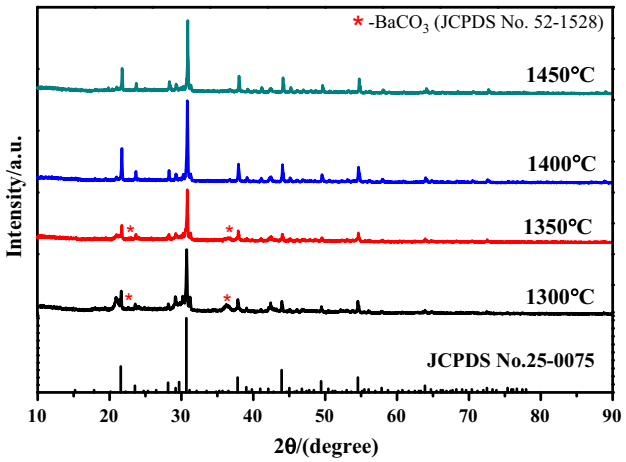

Figure 2 The XRD patterns of $Ba_3Al_2O_6$:0.06Eu^{3+} calcinated under different temperatures.

clearly in the detected region, which means that amorphous phase is predominant in this sample and the crystallinity is poor. With the increase of calcinations temperature, whole of the samples are converted into nanorods and the nanorods are straight in nature. What is more, lattice fringes become clearer. The formation of these varying morphologies is not yet well understood. As can be seen from Fig. 3d and e, the nanorods calcined at 1350 °C have the range of diameter 40–80 nm and length in the range from 2 to 8μm. HRTEM image shows very clear lattice fringes and the amorphous phase has disappeared (see Fig. 3f). The obvious lattice fringes confirm the high crystallinity of the sample calcined at 1350 °C. The interplanar spacing of lattice fringes is 0.317 nm, ascribed to (511) planes of $Ba_3Al_2O_6$. However, a part of lattice sites are not aligned or go right through the entire array, indicating the presence of defects in the crystal. For the samples calcined at 1400 and 1450 °C, the length of nanorods decreases to about 2–6μm and the diameter increases to 50–110 nm (see Fig. 3g, h, j, k). Further, HRTEM analysis reveals that the lattice fringes with the interplanar spacing of 0.333 and 0.441 nm are present and assigned to the (442) and (321) planes for the sample calcined at 1400 °C (see Fig. 3i). The orientations in different directions show the polycrystalline nature of sample [20]. While, as for the sample calcined at 1450 °C, only lattice fringes of (422) planes can be observed (see Fig. 3l), which means the sample is of single-crystalline nature. Therefore, it is concluded that the crystallinity increases with the increase of calcinations temperature, which is consistent with the XRD results. In general, all experimental results

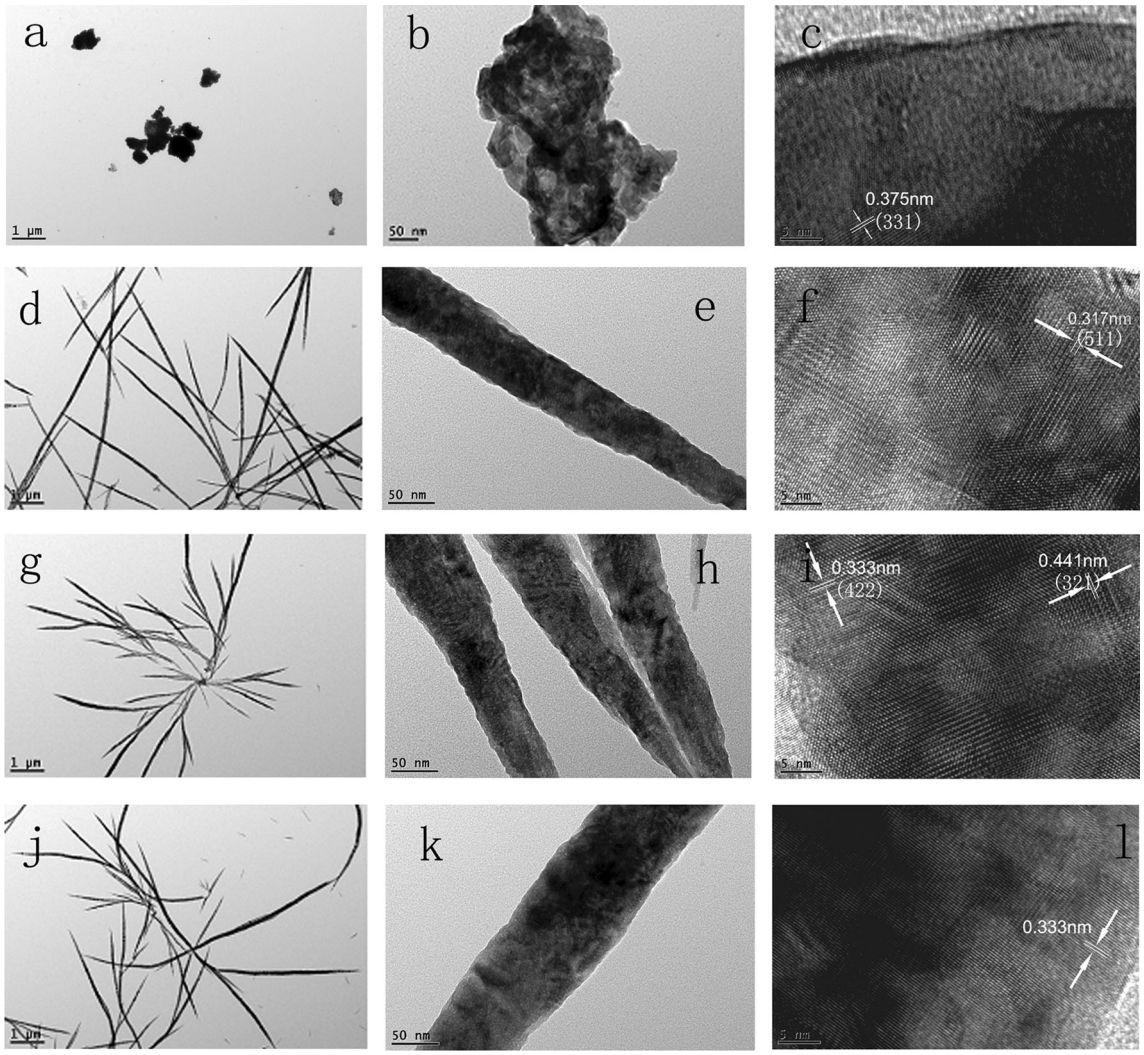

Figure 3 TEM and HRTEM micrographs of $Ba_3Al_2O_6$:0.06Eu^{3+} calcined at 1300 °C (**a**, **b**, **c**), 1350 °C (**d**, **e**, **f**), 1400 °C (**g**, **h**, **i**) and 1450 °C (**j**, **k**, **l**).

discussed above confirm that morphology and crystallinity of $Ba_3Al_2O_6$ are heavily affected by the calcination temperature.

Figure 4 shows the emission spectra excited at 394 nm for $Ba_3Al_2O_6$:0.06Eu^{3+} calcined at different temperatures. The emission intensity increases with the increase of calcination temperature. The reason may be due to the better crystallinity at higher calcination temperature, just as discussed above.

The effect of Eu^{3+} concentration on the photoluminescence properties of $Ba_3Al_2O_6$:Eu^{3+} samples

The XRD patterns of $Ba_3Al_2O_6$ samples doped with different Eu^{3+} concentrations are presented in Fig. 5. It is found that all the diffraction peaks of samples are in agreement with that of the standard card (JCPDS No. 25-0075) when the Eu^{3+} concentration (x) is lower than 0.04. Then the impurity phase $BaAl_2O_4$ (JCPDS No. 17-0306) appears when x exceeds 0.04 and the amounts of $BaAl_2O_4$ increase with the increase of Eu^{3+} concentration. Similar results are observed in rare earth-doped $Ca_3Al_2O_6$ phosphors [12]. This indicates that Eu^{3+} concentration has strong influence on the phase of synthesized $Ba_3Al_2O_6$ samples. Since the ionic radius of Eu^{3+} (0.095 nm) is smaller than that of Ba^{2+} (0.136 nm), the structure of $Ba_3Al_2O_6$ will be distorted when Eu^{3+} ions occupy the Ba^{2+} sites. According to the ratio of raw materials of $Ba_3Al_2O_6$:xEu, if Eu^{3+} replaces Ba^{2+}, it will lead to an excess of BaO and Al_2O_3 and the Al_2O_3 will react with

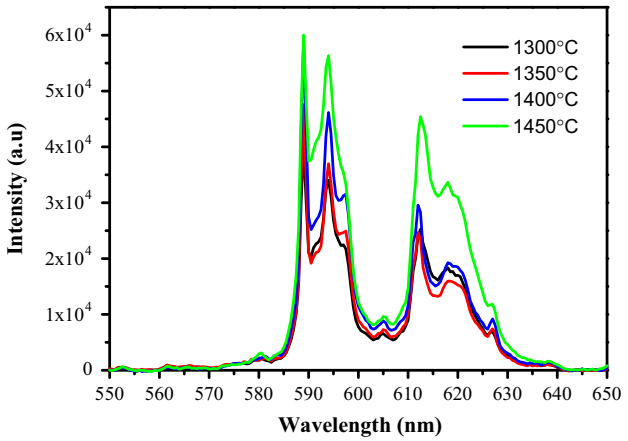

Figure 4 The emission spectra excited by 394 nm for the samples calcined at different temperatures.

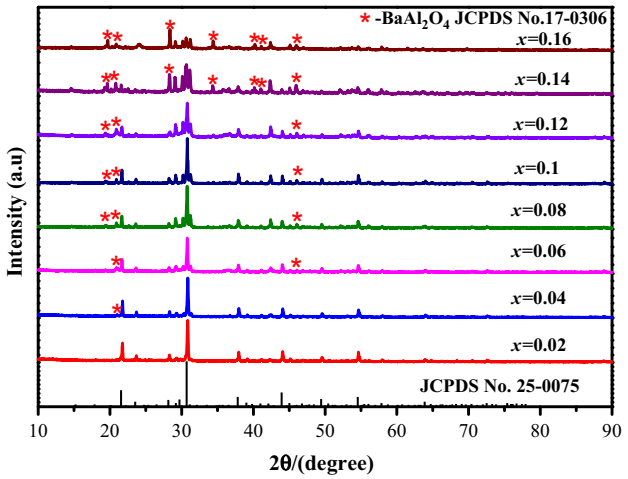

Figure 5 The XRD patterns of different Eu^{3+} concentration-doped $Ba_3Al_2O_6$:Eu^{3+} samples calcined at 1450 °C.

$Ba_3Al_2O_6$ to form $BaAl_2O_4$ [16, 21]. Usually, the diffraction peaks will move to the larger angles with increasing Eu^{3+} concentration when Ba^{2+} are replaced by the Eu^{3+} ions with smaller ionic radius. However, the diffraction peaks of samples move very slightly to the low-angle side with increase of Eu^{3+} concentration, demonstrating the increase of lattice constant in the samples [22, 23]. The reason may be that some Eu^{3+} ions are incorporated into the interstitial sites of crystal.

Figure 6 presents emission spectra of different Eu^{3+} concentration-doped $Ba_3Al_2O_6$ samples calcined at 1450 °C under 394 nm excitation. It can be seen that photoluminescence intensity of $^5D_0 \rightarrow {}^7F_1$ transition (589 nm) grows with increasing Eu^{3+}

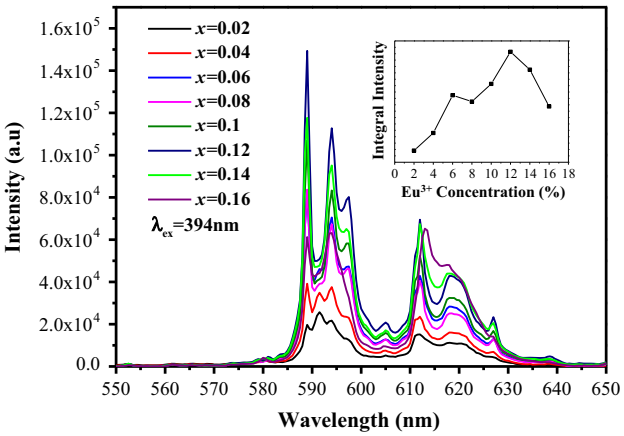

Figure 6 Emission spectra of different Eu^{3+} concentration-doped $Ba_3Al_2O_6$ samples under 394 nm excitation. The inset shows the dependence of integral intensity on the Eu^{3+} concentration.

concentration up to $x = 0.12$. Further increase of Eu^{3+} concentration leads to intensity reduction because of concentration quenching. This quenching process is often attributed to energy migration among the Eu^{3+} ions. As the Eu^{3+} concentration increases, the distance between Eu^{3+} ions become shorter which may lead to growing energy migration between activator centres and thus enhanced probability of reaching a luminescence-killing defect [24, 25]. This optimal concentration of Eu^{3+} ions in $Ba_3Al_2O_6$ samples is lower than those in other aluminate hosts, such as YAG and $SrAl_2O_4$ [26, 27]. Eu^{3+} ion is known as a sensitive probe for the site symmetry. The red emission $^5D_0 \rightarrow {}^7F_2$ transition is highly sensitive to the environment symmetry and a larger probability of this transition will be increased due to a decrease in symmetry. However, $^5D_0 \rightarrow {}^7F_1$ transition hardly varies with the crystal field strength around Eu^{3+} ions and can be taken as a Ref. [28]. Therefore, the ratio of emission intensity of $^5D_0 \rightarrow {}^7F_2$ transition to that of $^5D_0 \rightarrow {}^7F_1$ transition, known as asymmetry factor R, is used to be a criterion for the site symmetries of Eu^{3+} ions. Generally, R is <1.0 for symmetric and >1.0 for noncentrosymmetric surroundings [29]. Figure 7 shows the dependence of asymmetry factor R on the Eu^{3+} concentration under 394 nm excitation wavelength in $Ba_3Al_2O_6$ samples. The R value is <1.0 and decreases with increase of Eu^{3+} concentration when x is lower than 0.12, which confirms that the Eu^{3+} ions are located in a symmetric environment, while the R values show an increasing tendency when Eu^{3+} concentration x

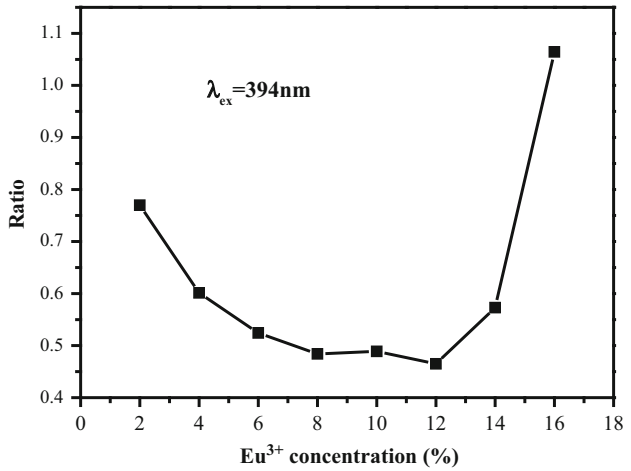

Figure 7 Dependence of asymmetry factor R on the Eu^{3+} concentration under 394 nm excitation wavelength.

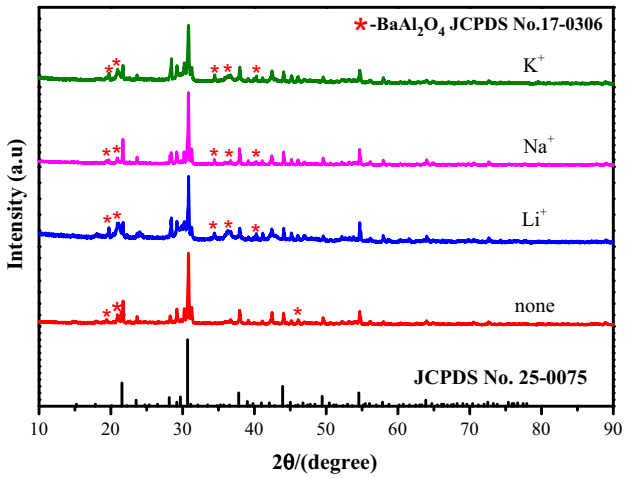

Figure 8 The XRD patterns of $Ba_3Al_2O_6$:0.06Eu^{3+} samples doped with different charge compensators.

exceeds 0.12, which means the decrease of local symmetry of Eu^{3+} ions. The reason is possible that the ion radius of Eu^{3+} is much smaller than that of Ba^{2+} ion. When Eu^{3+} ions enter the host lattice and substitute Ba^{2+} ions, barium vacancies are produced in order to keep charge balance in the materials, $Eu_2O_3 \longrightarrow Ba_3Al_2O_6 2Eu_{Ba} + V''_{Ba} + 3O_0$. These defects will lead to the distortion of local environment symmetries of Eu^{3+} ions [30]. With the increase of Eu^{3+} concentration, more barium vacancies are induced, leading to lowering the symmetry of the surrounding Eu^{3+} ions [31]. For the sample in which Eu^{3+} concentration $x = 0.16$, the R value increases abruptly and is found to be 1.06, so the Eu^{3+} ions located in asymmetric environment are predominant. We think that impurity phase $BaAl_2O_4$ makes a great contribution to the R value. With the increase of Eu^{3+} concentration, the impurity phase cannot be negligible and Eu^{3+} ions may incorporate into $BaAl_2O_4$ host, so the real Eu^{3+} concentration doped into $Ba_3Al_2O_6$ samples maybe lower than that expected. On the other hand, the red emission of $^5D_0 \rightarrow {}^7F_2$ transition is predominant in the Eu^{3+}-doped $BaAl_2O_4$ phosphors because the Eu^{3+} ions occupy the barium sites with low symmetry [28]. Therefore, emission intensity of $^5D_0 \rightarrow {}^7F_1$ transition (589 nm) decreases and that of $^5D_0 \rightarrow {}^7F_2$ transition (612 nm) increases in high Eu^{3+} concentration-doped samples, and then intensity ratio of $^5D_0 \rightarrow {}^7F_2$ transition to that of $^5D_0 \rightarrow {}^7F_1$ transition increases according to the analysis above. This assumption can be proved by the emission spectrum of the sample in which Eu^{3+} concentration $x = 0.16$. It can be seen that the profile of the emission spectrum is different than those in other Eu^{3+} concentration-doped samples and the peak of $^5D_0 \rightarrow {}^7F_2$ transition shifts from 612 to 613 nm. So we think the emission spectrum is an overlap of those in $Ba_3Al_2O_6$ and $BaAl_2O_4$ hosts.

The effect of charge compensators on the photoluminescence properties of $Ba_3Al_2O_6$:0.06Eu^{3+}

The replacement of divalent Ba^{2+} ion by trivalent Eu^{3+} ion will produce defects in the crystal lattice, so Li^+, Na^+ and K^+ are often introduced as charge compensator to reduce the distortion of local environment symmetries of optical centres caused by the defects and enhance the overall photoluminescence intensity [30]. Figure 8 shows the XRD patterns for $Ba_3Al_2O_6$:0.06Eu^{3+} calcined at 1450 °C and its charge compensated (with Li^+, Na^+, K^+ ions) counterparts. The XRD patterns show that $Ba_3Al_2O_6$ is predominant in the samples. However, the impurity phase $BaAl_2O_4$ will increase in the charge compensator co-doped samples comparing with those without charge compensators.

Figure 9 shows the emission spectra of the samples under 394 nm excitation. The shapes of the emission spectra of all the samples are very similar, indicating that the introduction of charge compensators (Li^+, Na^+, K^+ ions) does not change the sublattice structure around the luminescent centre of Eu^{3+} ions [32]. However, the emission intensities of

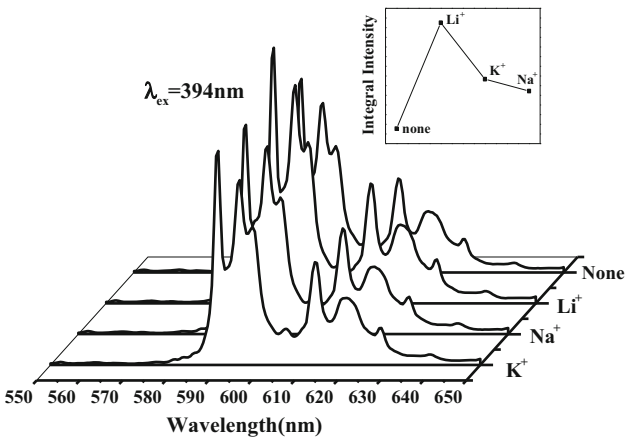

Figure 9 The emission spectra of $Ba_3Al_2O_6$:0.06Eu^{3+} samples doped with different charge compensators under 394 nm excitation.

$^5D_0 \rightarrow {}^7F_1$ transition are significantly enhanced by the addition of charge compensators. In the Eu^{3+}-doped $Ba_3Al_2O_6$ host, not all Eu^{3+} ions go into the lattice and occupy Ba^{2+} sites, instead impurity phases Eu_2O_3 or BaO may exist in the samples because of the charge imbalance caused by the substitution of divalent Ba^{2+} ion with trivalent Eu^{3+} ion. The existence of Eu_2O_3 or BaO could restrain the $Ba_3Al_2O_6$ grains growth during the sintering process, leading to the decrease in emission intensity [32]. The addition of charge compensator can help to incorporate Eu^{3+} ions into Ba^{2+} sites by compensating the different charges between Eu^{3+} and Ba^{2+} ions. So the emission intensity can be enhanced. Furthermore, the emission intensity depended on the type of charge compensator. The inset in Fig. 9 shows the dependence of integral intensity of $^5D_0 \rightarrow {}^7F_1$ transition on the type of charge compensator. The emission intensity of the sample with Li^+ as the charge compensator is higher than those of samples co-doped with Na^+, Eu^{3+} and K^+, Eu^{3+}. The reason is that Li^+ ions are easier to enter into the interstitial site of $Ba_3Al_2O_6$ crystal lattice than the others and introduces the smaller lattice distortions, because the ionic radius of Li^+ (0.076 nm) is smaller than those of Na^+ (0.102 nm) and K^+ (0.138 nm) [5, 33]. However, the emission intensity of the sample co-doped with Na^+, Eu^{3+} is lower than that co-doped with K^+, Eu^{3+}, which is contrary to the results obtained in $ZnMoO_4$ and $CaBO_3Cl$ hosts [32, 33]. The reason is possible that the ionic radius of K^+ is similar to that of Ba^{2+} (0.136 nm), so K^+ ion is easier to substitute Ba^{2+} ion than Na^+ ion.

Conclusions

Eu^{3+}-doped $Ba_3Al_2O_6$ phosphors are synthesized by high-temperature solid-state method. The influence of calcinations temperature, Eu^{3+} concentration as well as charge compensators on the crystal structure, morphology and photoluminescence properties is investigated. The XRD analysis confirms that cubic phase $Ba_3Al_2O_6$ is predominant in the as-prepared samples. The crystal structure is not changed in the four samples calcined at different calcination temperatures and those co-doped with charge compensators. However, the impurity phase $BaAl_2O_4$ is obtained in the high Eu^{3+} concentration-doped samples. The morphology of the sample depends on the calcination temperature heavily. The particles are converted into nanorods when the calcination temperature exceeds 1350 °C. The photoluminescence spectra studies reveal a strong peak at 589 nm due to $^5D_0 \rightarrow {}^7F_1$ transition of Eu^{3+} ions, when excited at 394 nm. The emission shows an increase in intensity with increasing calcinations temperature from 1300 to 1450 °C. The optimum Eu^{3+} concentration is about 12 % for the sample calcined at 1450 °C. The emission intensity can be significantly enhanced by the addition of charge compensators. The sample doped with Li^+ as charge compensator exhibits the strongest emission intensity. Therefore, $Ba_3Al_2O_6$:Eu^{3+} phosphors with charge compensator are potential candidates for UV-excited WLEDs.

Acknowledgements

This work has been supported by Natural Science Foundation of China (51304086), pilot funding of rare earth development and application of Ganzhou, the Leading Academic Discipline Project of Jiangxi University of Science and Technology.

References

[1] Li H, Jia Y, Sun W, Zhao R, Fu J, Jiang L, Zhang S, Pang R, Li C (2014) Novel energy transfer mechanism in single-phased color-tunable Sr_2CeO_4:Eu^{3+} phosphors for WLEDs. Opt Mater 36:1883–1889

[2] Zhu H, Lin CC, Luo W, Shu S, Liu Z, Liu Y, Kong J, Ma E, Cao Y, Liu R, Chen X (2014) Highly efficient non-rare-earth red emitting phosphor for warm white light-emitting diodes. Nat Commun 5:4312

[3] Mao Z, Zhu Y, Wang Y, Gan L (2014) Ca_2SiO_4:Ln (Ln = Ce^{3+}, Eu^{2+}, Sm^{3+}) tricolor emission phosphors and their application for near-UV white light-emitting diode. J Mater Sci 49:4439–4444. doi:10.1007/s10853-014-8140-4

[4] Bandi VR, Grandhe BK, Jang K, Lee HS, Shin DS, Yi SS, Jeong JH (2012) Citric based sol-gel synthesis and luminescence characteristics of $CaLa_2ZnO_5:Eu^{3+}$ phosphors for blue LED excited white LEDs. J. Alloys Compd 512:264–269

[5] Wang T, Xu X, Zhou D, Qiu J, Yu X (2014) Red phosphor $Ca_2Ge_7O_{16}:Eu^{3+}$ for potential application in field emission displays and white light-emitting diodes. Mater Res Bull 60:876–881

[6] Salimi R, Sameie H, Sabbagh Alvani AA, Sarabi AA, Moztarzadeh F, Eivaz Mohammadloo H, Nargesian F, Tahriri M (2012) Sol–gel synthesis, structural and optical characteristics of $Sr_{1-x}Zn_2Si_{2y}O_{7+\delta}$:$xEu^{2+}$ as a potential nanocrystalline phosphor for near-ultraviolet white light-emitting diodes. J Mater Sci 47:2658–2664. doi:10.1007/s10853-011-6091-6

[7] Suresh K, Poornachandra Rao NV, Murthy KVR (2014) Photoluminescent properties of $Sr_2CeO_4:Eu^{3+}$ and $Sr_2CeO_4:Eu^{2+}$ phosphors suitable for near ultraviolet excitation. Bull Mater Sci 37:1191–1195

[8] Chen W, Wang Y, Xu X, Zeng W, Gong Y (2012) A new long-lasting phosphor Ce^{3+} doped $Ca_3Al_2O_6$. ECS Sol State Lett 1:R17–R19

[9] Lazic B, Kahlenberg V, Kaindl R, Kremenovic A (2009) On the symmetry of $Ba_3Al_2O_6$—X-ray diffraction and Raman spectroscopy studies. Sol State Sci 11:77–84

[10] Chang C, Li W, Huang X, Wang Z, Chen X, Qian X, Guo R, Ding Y, Mao D (2010) Photoluminescence and afterglow behavior of Eu^{2+}, Dy^{3+} and Eu^{3+}, Dy^{3+} in $Sr_3Al_2O_6$ matrix. J Lumin 130:347–350

[11] Ju H, Deng W, Wang B, Liu J, Tao X, Xu S (2012) The structure and luminescence properties of green $Ca_3Al_2O_6$:-Bi^{3+} phosphors. J Alloys Compd 516:153–156

[12] Zhang J, He Y, Qiu Z et al (2014) Site-sensitive energy transfer modes in $Ca_3Al_2O_6:Ce^{3+}/Tb^{3+}/Mn^{2+}$ phosphors. Dalton Trans 43:18134–18145

[13] Guo X, Lei L, Lv C, Sun Y, Zheng H, Cui Y (2008) Preparation and photoluminescence property of a loose powder, $Ca_3Al_2O_6:Eu^{3+}$ by calcination of a layered double hydroxide precursor. J Sol State Chem 181:1776–1781

[14] Yerpude AN, Dhoble SJ (2012) Luminescence properties of micro $Ca_3Al_2O_6:Dy^{3+}$ phosphor. Micro Nano Lett 7:268–270

[15] Zhang J, Zhang X, Shi J, Gong M (2011) Luminescent properties of green- or red-emitting Eu^{2+}-doped $Sr_3Al_2O_6$ for LED. J Lumin 131:2463–2467

[16] Li G, Lai Y, Cui T, Yu H, Liu D, Gan S (2010) Luminescence properties and charge compensation of $Sr_3Al_2O_6$ doped with Ce^{3+} and alkali metal ions. Mater Chem Phys 124:1094–1099

[17] Wang L, Guo H, Wei Y, Noh HM, Jeong JH (2015) White luminescence and energy transfer process in Bi^{3+}, Sm^{3+} co-doped $Ca_3Al_2O_6$ phosphors. Opt Mater 42:233–236

[18] Wani JA, Dhoble NS, Kokode NS, Deva Prasad Raju B, Dhoble SJ (2014) Synthesis and luminescence property of $Li_2BaP_2O_7:Ln^{3+}$ (Ln = Eu, Sm) phosphors. J Lumin 147:223–228

[19] Kolesnikov IE, Tolstikova DV, Kurochkin AV, Pulkin SA, Manshina AA, Mikhailov MD (2015) Concentration effect on photoluminescence of Eu^{3+}-doped nanocrystalline YVO_4. J Lumin 158:469–474

[20] Nagabhushana H, Sunitha DV, Sharma SC, Daruka Prasad B, Nagabhushana BM, Chakradhar RPS (2014) Enhanced luminescence by monovalent alkali metal ions in Sr_2SiO_4:-Eu^{3+} nanophosphor prepared by low temperature solution combustion method. J Alloys Compd 595:192–199

[21] Jiang W, Fu R, Gu X, Zhang P, Cosgun A (2015) A red-emitting phosphor $LaSr_2AlO_5:Eu^{3+}/Eu^{2+}$ prepared under oxidative and reductive atmospheres. J Lumin 157:46–52

[22] Song X, Fu R, Agathopoulos S, He H, Zhao X, Zhang S (2009) Photoluminescence properties of Eu^{2+}-activated $CaSi_2O_2N_2$ Redshift and concentration quenching. J Appl Phys 106:033103-1–033103-5

[23] Shimokawa Y, Sakaida S, Iwata S, Inoue K, Honda S, Iwamoto Y (2015) Synthesis and characterization of Eu^{3+} doped $CaZrO_3$-based perovskite type phosphors. Part II: PL properties related to the two different dominant Eu^{3+} substitution sites. J Lumin 157:113–118

[24] Huang J, Yi S, Deng Y, Xian J, Zhang L (2015) A novel red emitting phosphor of Eu^{3+} doped $Sr_2La_2MgW_2O_{12}$ for white light emitting diodes, Spectrochim. Acta Part A 148:324–327

[25] Sheetal Taxak VB, Arora R, Dayawati Khatkar SP (2014) Synthesis, structural and optical properties of $SrZrO_3:Eu^{3+}$ phosphor. J Rare Earths 32:293–297

[26] Kolesnikov IE, Tolstikova DV, Kurochkin AV, Manshina AA, Mikhailov MD (2014) Eu^{3+} concentration effect on luminescence properties of YAG:Eu^{3+} nanoparticles. Opt Mater 37:306–310

[27] Fu Z, Ma L, Sahi S, Hall R, Chen W (2013) Influence of doping concentration on valence states of europium in $SrAl_2O_4$ Eu phosphors. J Lumin 143:657–662

[28] Bandi VR, Jayasimhadri M, Jeong J, Jang K, Lee HS, Yi SS, Jeong JH (2010) Host sensitized novel red phosphor $CaZrSi_2O_7:Eu^{3+}$ for near UV and blue LED-based white LEDs. J Phys D 43:395103-1–395103-7

[29] Chengaiah T, Jamalaiah BC, Rama Moorthy L (2014) Luminescence properties of Eu^{3+}-doped $Na_3Gd(PO_4)_2$ red-emitting nanophosphors for LEDs, Spectrochim. Acta Part A 133:495–500

[30] Puchalska M, Zych E, Sobczyk M, Watras A, Deren P (2014) Effect of charge compensation on up-conversion and UV excited luminescence of Eu^{3+} in Yb^{3+}–Eu^{3+} doped calcium aluminate $CaAl_4O_7$. Mater Chem Phys 147:304–310

[31] Suresh Kumar A, Arun Kumar R, Balasundaraprabhu R, Senthil K, Ramesh Kumar S, Gunasekaran V (2015) Influence of calcination temperature on the luminescent properties of Eu^{3+} doped $CaAl_4O_7$ phosphor prepared by Pechini method, Spectrochim. Acta Part A 134:283–287

[32] Xie A, Yuan X, Wang F, Shi Y, Mu Z (2010) Enhanced red emission in ZnMoO4:Eu3+ by charge compensation. J Phys D 43:055101-1–055101-5

[33] Yang F, Liang Y, Liu M, Li X, Wang N, Xia Z (2012) Enhanced red-emitting by charge compensation in Eu^{3+}-activated Ca_2BO_3Cl phosphors. Ceram Int 38:6197–6201